

Recognition from Hand Cameras

Cheng-Sheng Chan, Shou-Zhong Chen, Pei-Xuan Xie, Chiung-Chih Chang, Min Sun
National Tsing Hua University

{s104061526@m104, s104061545@m104, s101061230@m101, s101060006@m101, sunmin@ee}.nthu.edu.tw

Abstract

We propose *HandCam* (Fig. 1), a novel wearable camera capturing activities of hands, for recognizing human behaviors. *HandCam* has two main advantages over egocentric systems [10, 5, 23]: (1) it avoids the need to detect hands and manipulation regions; (2) it observes the activities of hands almost at all time. These nice properties enable *HandCam* to recognize hand states (free v.s. active hands, hand gestures, object categories), and discover object categories through interaction with hands. We propose a new method to accomplish these tasks by fusing per-frame state prediction with state changes estimation from a pair of frames. We have collected one of the first *HandCam* dataset with 20 videos captured in three scenes. Experiments show that *HandCam* system significantly outperforms a state-of-the-art *HeadCam* system (frame-based re-implementation similar to [17]) in all tasks by at most 10.8% improvement in accuracy. We also show that *HandCam* videos captured by different users can be easily aligned to improve free v.s. active recognition accuracy (3.3% improvement) in cross-scenes use case. Moreover, we observe that finetuning Convolutional Neural Network [14] consistently improves accuracy (at most 4.9% better). Finally, a method combining *HandCam* and *HeadCam* features achieves the best performance. With more data, we believe a joint *HandCam* and *HeadCam* system can robustly log hand states in daily life.

1. Introduction

The recent progress of wearable devices has led to a significant interest in recognizing human behaviors in daily life (i.e., uninstrumented environment). Among many devices, egocentric camera systems have drawn significant attention, since the camera is aligned with the wearer’s field-of-view, it naturally captures what a person sees. These systems have shown great potential in recognizing daily activities (e.g., making meals, watching TV, etc.) [22], estimating hand poses [23, 24], generating how-to videos [5], etc.

Despite many advantages of egocentric camera systems, there exists two main issues which are much less discussed [23]. Firstly, hand localization is not solved especially

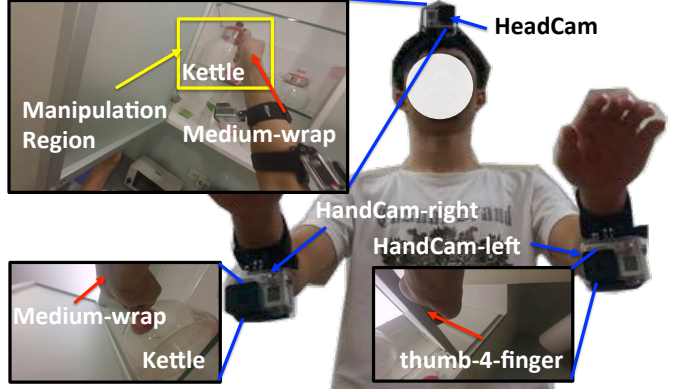


Figure 1: Illustration of our wearable camera system: consisting of three wide-angle cameras, two mounted on the left and right wrists to capture hands (referred to as *HandCam*) and one mounted on the head (referred to as *HeadCam*). We use our *HandCam* system to robustly recognize object categories (see yellow boxes for illustration) and hand gestures (see red arrows for illustration).

for passive camera systems. Even for active camera systems like Kinect, hand localization is challenging when two hands are interacting or a hand is interacting with an object. Secondly, a limited field-of-view of an egocentric camera causes hands to frequently move outside the images. This restricts the egocentric approaches to focus on recognizing activities which require continuous hand-eye coordination. On the other hand, cameras have been mounted on other locations to avoid similar issues. In project Digit [13], a camera is mounted on a user’s wrist to always observe the user’s hand pose. This allows a user to issue gesture commands at any time. Similarly, a camera has been mounted on a robot arm for accurately picking up an object [25]. Hence, we argue that egocentric camera system might not be the best wearable system for recognizing human behaviors.

To address these issues, we propose a novel wearable system with cameras on wrists to capture both hands (Fig. 1). We name our system “*HandCam*” which is dramatically different from egocentric systems with cameras on head or chest (e.g., [10, 5, 23]). By wearing cameras on wrists, our system directly recognizes the states of hands (e.g., object: kettle; gesture: medium-wrap in Fig. 1). It avoids the needs to detect hands and infer manipulation re-

gions as required in classical egocentric systems [10]. We propose a novel method to classify hand states including free v.s. active (i.e., hands holding objects or not), object categories, and hand gestures (Sec. 3.3). A similar method is also proposed to discover object categories in an unseen scene (Sec. 3.7). Both methods incorporate per-frame visual information to predict states and pairwise change information of a pair of nearby frames to predict state changes. By combining these information, we achieve the best state classification accuracy.

To evaluate our system, we collected one of the first HandCam dataset. The dataset consists of 20 sets of video sequences (i.e., each set includes two HandCams and one HeadCam synchronized videos) captured in three scenes: a small office, a mid-size lab, and a large home. In order to thoroughly analyze recognition tasks, we ask users to interact with multiple object categories and multiple object instances. We also ask multiple users to wear our system in a casual way to consider the variation introduced by multiple users. To overcome this variation, a fully automatic hand alignment method is proposed (Sec. 3.2).

Experiments show that our HandCam system significantly outperforms a state-of-the-art HeadCam system (frame-based re-implementation similar to [17]) in all tasks by at most 10.8% improvement in accuracy. Moreover, we show that HandCam videos captured by different users can be easily aligned to improve free v.s. active recognition accuracy (3.3% acc. improvement) in cross-scenes use case. In all experiments, we use state-of-the-art Convolutional Neural Network (CNN)[14] features. We observe that fine-tuning CNN consistently improves accuracy (at most 4.9% improvement). Finally, a method combining HandCam and HeadCam features achieves the best performance.

2. Related Work

In this section, we review related work in egocentric recognition, hand detection and pose estimation, and a few works inspired our HandCam system.

2.1. Egocentric Recognition

[10, 7, 9] are the early egocentric works learning to recognize objects, object states, actions, and activities. These methods assume foreground objects and hands can be easily separated from background using appearance, geometric, and motion cues. Their methods are evaluated on an egocentric activity dataset where the users move mainly their hands in front of a static table. [22] proposes to recognize activities through recognizing objects in the field-of-view. The method is evaluated on a dataset with many long-length videos of daily activities. Since their approach is based on objects in the field-of-view, it may confuse with activities co-occurred at the same place. In this work, we allow users to naturally move to different places in a scene, which creates addition challenge for egocentric system to localize hands. However, since our HandCam significantly reduces

hand location variation (Fig. 2(a)), this scenario won't be an issue for our HandCam system.

[8, 17, 18] further show the importance of gaze to help recognizing actions requiring "hand-eye coordination". We argue that not all daily activities consistently requires hand-eye coordinate. For instance, grasping one's wallet from one's pocket do not require hand-eye coordination. In such cases, head movement and gaze information might be misleading, and the user's hand and object of interest might not even been captured in the field-of-view of the egocentric camera (Fig. 2(b)). On the other hand, our HandCam system consistently captures hand-object interaction at all time for a variety of daily activities. Finally, a few works [11, 19, 26] focus on summarizing egocentric videos by recognizing objects, people, and scenes.

Extra sensors. [6] utilizes motion capture techniques, static cameras, wearable IMUs, and a head-mounted camera to study food preparation process in an instrumented kitchen. [5] proposes to combine egocentric camera with gaze tracker to robustly "discover" objects of interest given multiple sequences recorded in the same scene conducting the same tasks by different subjects. [20] proposes to use a head-mounted RGBD camera to recognize both manipulation and non-manipulation activities. [4] also proposes to use RGBD camera to model background and "discover" foreground objects. In this work, we show that with our HandCam system, objects can also be discovered without the need of additional gaze tracker or RGBD sensor (Sec. 3.7).

2.2. Hand Detection and Pose Estimation

[23, 24] focus on estimating 3D hand poses using wearable RGBD camera. Despite many success in 3D hand pose recognition, [23] shows that egocentric 3D hand poses estimation is very challenging due to common interaction between hands and other objects or scene elements. [16, 15] focus on detecting hand pixels in RGB images while users are moving around various environments. [1] studies the weakness of [16] and proposes method for reducing false positive detection of hands. Although these RGB methods are not as robust as RGBD methods, these methods have been applied to discover hand gestures [12].

2.3. Camera for Hands

A few work have proposed to wear cameras on wrists or other body parts to recognize gestures, poses, and activities of hands. In [13, 28], cameras are mounted on a user's wrists to always observe user's hand pose. This allows a user to issue gesture commands at any time. However, the project assumes that a user is hand free of objects. In contrast, our HandCam system focuses on recognizing hand-object interactions. Similarly, a camera has been mounted on a robot arm for it to accurately pick up an object [25]. Although the robot has other sensors like a stereo camera and a lazer range finder which are not mounted on the robot

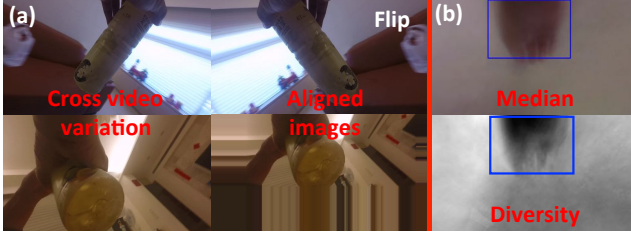


Figure 3: Cross-videos Hand Alignment. Panel (a)-left shows the cross-video hand variation. Panel (a)-right shows flipped and multi-scale template aligned images. Panel (b) shows example of median and diversity images on the top and bottom, respectively.

arm, it has been shown that the HandCam is essential for picking up an object. [3] recently propose to wear a camera on hand webbings to recognize hand gestures and context-aware interactions such as events triggered by object recognition. However, they assume that objects are instrumented with QR codes. These works suggest that egocentric camera system might not be the best wearable system for understanding human behaviors. [21] is a recent paper that achieves an outstanding recognition accuracy using a wrist mounted camera (only on right hand) instead of a head mounted camera. They directly recognize 23 classes of activities of daily life without explicitly recognizing object categories and gestures. In their experiments, they assume that the temporal segment of each action is given. Hence, per-segment classification accuracy is evaluated, whereas per-frame classification accuracy is evaluated in this paper.

3. Our System

Our wearable camera system (Fig. 1) consists of three wide-angle cameras. Two HandCams are positioned toward the left and right palms to have a stable view of everything interacting with the hand. The third HeadCam serves as a classical egocentric system for comparison and is shown to be complementary to HandCam in Sec. 3.8.

3.1. Wearable Cues

The strength of a wearable system essentially lies in the unique cues it can extract. For an egocentric system, these cues include gaze, hand, and foreground information. Some systems utilize active sensors to reliably localize hands (e.g., RGBD sensor in [24]) or predict user’s attention (e.g., gaze tracker in [5]). However, they require extra hardware expenses and more power consumption. Many other egocentric systems require only a camera. However, sophisticated pre-processing steps [10, 7, 18, 17] are required for removing irrelevant information in background.

Our HandCam system is designed with two focuses:

- **Stable Hand Cue.** Significantly reduced hand location variation (Fig. 2(a)-bottom) as compared to egocentric systems which have larger hand location variation (Fig. 2(a)-top). Our system also won’t be confused between left and right hands, since they are recorded by

different cameras. Instead, we augment our dataset by flipping left hand images to mimic right hand images.

- **Always Observed.** Almost all hand related activities are observed as compared to egocentric systems which have limited field-of-view that missed many hand related activities (Fig. 2(b)).

Human factors. As we design our system to be used by general users, we let each user to wear the system only under a general guideline. As a consequence, different users mount the camera with different distances and orientation. Therefore, the hand location variation “across” video sequences (Fig. 3(a)-left) is noticeable. However, once the camera is mounted on a user’s wrists, it is true that the spatial variation of hand regions are small within the video. By utilizing this fact, we propose a fully automatic cross-videos hand alignment method.

3.2. Hand Alignment

In each video sequence, we model the pixel value (i.e., a value between 0 ~ 255) distribution across time for each pixel and each color channel as a Laplace distribution parameterized by center (μ) and diversity (β). We estimate the parameters of the distribution using maximum likelihood estimators, where the median image represents the common pattern (Fig. 3(b)-top) and the diversity image represents the variation of pixel values (black indicates small variation in Fig. 3(b)-bottom). We simply treat the regions with diversity β smaller than β_{th} for all color channel as “stable” hand mask (within blue box in Fig. 3(b)-bottom). We find the video with the smallest “stable” hand mask region as the reference video, and use the median of the region as alignment template (blue box in Fig. 3(b)-top).

Multiscale alignment. We apply multiscale normalized cross-correlation to align the template to the median image of every other video. Next, we transform all median images to the coordinate of the reference video and define the “reference image region” as the median of the top-left and the bottom-right corners of all transform images.

Aligned images. We transform the reference image region back to the coordinate system of each video. Then, we apply cropping and replicate padding to generate hand aligned images (Fig. 3(a)-right).

3.3. Hand States Recognition

Given the aligned sequences (Fig. 3(a)-right) and always observed hand activities (Fig. 2(b)-bottom), we propose to recognize the states of hands for multiple tasks (Fig. 4).

Free v.s. active. The most fundamental states of interests is to recognize whether the hand is interacting with an object (referred to as “active state”), or not (referred to as “free state”). In this work, we explicitly evaluate the performance of active hands recognition undergoing some unseen activities.

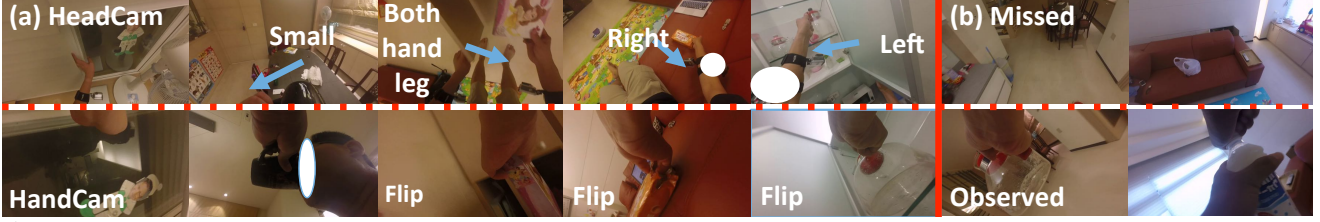


Figure 2: HandCam (bottom-row) v.s. HeadCam (top-row). Panel (a) compares the hand location variation. The variation in HandCam (bottom) is significantly less than variation in HeadCam (top). We also know exactly which video captures left or right hand. Hence, we always flip left hand images to mimic right hand images. Panel (b) shows typical examples of missed hands in HeadCam but observed hands in HandCam. We block some parts of the image to avoid privacy concerns.



Figure 4: Typical hand states in HandCam view: object category (top-white-font) and hand gesture (bottom-red-font). The statistics of states in our dataset is shown in Table. 7

Hand gesture recognition. At a slightly finer level of granularity (12 gesture classes), we propose to recognize hand gestures in active state. Note that gesture is an important affordance cue for recognizing activities without the need to recognize a large number of object categories involving in the same activity.

Object category recognition. At the finest level of granularity (23 object categories), we propose to recognize object categories which have been interacted by hands. Categorical recognition allows our system to recognize an unseen object instance within a known category.

We take a fully supervised approach and train a frame-based multi-class state classifier. The classifier generates a confidence $u(s_i)$ for state s_i in the i^{th} frame. For example, $u(Active_i)$ specifies the confidence that the i^{th} frame contains an active hand. We take advantage of the recent breakthrough in deep learning and extract frame-based feature f_i from Convolutional Neural Network (CNN) [14], where i denotes the frame index. We describe the setting of the CNN model that we used in our application in Sec. 3.6.

3.4. State Change Detection

Since frame-based state recognition inevitably will contain spurious error predictions, we propose to restrict the locations of possible state changes by learning to detect them.

Frame-based change. We train a frame-based binary state change classifier (i.e., change or no change) by treating frames within d frames distance away from a ground truth change frame as positive examples and remaining frames as negative examples. The large value of d will increase the number of positive examples, but decreasing the localiza-

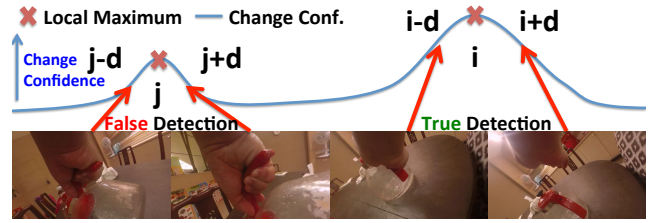


Figure 5: Illustration of state change detection. Two change candidates are shown, where the first one corresponds to a false detection and the second one corresponds to a true detection. Our system ensures high recall of state changes at this step.

tion ability of the true change locations. In order to reduce the visual variation of changes, we propose the following feature,

$$cf_i = |f_{i-d} - f_{i+d}| = |f_{i+d} - f_{i-d}|. \quad (1)$$

Intuitively, transition from active to free should have a similar feature representation as transition from free to active. Then, we can apply the change classifier to obtain frame-based state change confidences $\{b_i\}_i$ for all frames (Fig. 5).

Change candidates. Similar to classical edge detection [2], we need to remove redundant change candidates with high confidences. Hence, we apply non-maximum suppression to find local maximum with respect to state change confidences $\{b_i\}_i$ (Fig. 5). We define their locations and confidences as change candidates $\{(i, b_i)\}_{i \in C}$, where C contains a set of local maximum change locations. Note that we prefer high recall (more change candidates) at this step.

3.5. Full Model

We now combine frame-based state classification with detected change candidates to improve the classification of states. Both information are captured into a pairwise scoring function below,

$$R(S) = \sum_{i=1}^N u(s_i) + \lambda \sum_{i=1}^{N-1} \hat{b}(s_i, s_{i+1}), \quad (2)$$

where $R(S)$ is the score as a function of a set of states $S = [s_1, s_2, \dots, s_i, \dots, s_N]$, i is the index of frame, $s_i \in \{state1, state2, \dots\}$ is the state of the i^{th} frame, N is the

total number of frames, λ is the weight that balances the potentials, and $u(\cdot), \hat{b}(\cdot)$ are the unary and binary scoring functions, respectively.

Scoring functions. The unary scoring function is exactly the same as the scores in Sec. 3.3. The binary scoring function is defined below,

$$\hat{b}(s_i \neq s_{i+1}) = -\inf \text{ and } \hat{b}(s_i = s_{i+1}) = 0 \text{ if } i \notin C, \quad (3)$$

which means no change exists when the i^{th} frame is not a change candidate;

$$\hat{b}(s_i \neq s_{i+1}) = -S(\bar{f}_i, \bar{f}_{i+1}) \text{ and} \quad (4)$$

$$\hat{b}(s_i = s_{i+1}) = S(\bar{f}_i, \bar{f}_{i+1}) \text{ if } i \in C, \quad (5)$$

where $S(\bar{f}_i, \bar{f}_{i+1})$ is the cosine similarity between \bar{f}_i, \bar{f}_{i+1} , and \bar{f}_i is the average frame-based features between two consecutive candidate change frames. We apply a dynamic programming inference procedure to predict the states maximizing the score $R(S)$.

3.6. Deep Feature

Based on the Alexnet CNN architecture, we address the following questions: (1) which layer should we extract feature? and (2) will finetuning improve recognition from our novel HandCam point of view? We found that a compact six layers model achieves the best accuracy, while being more computationally efficient than the original Alexnet (Appendix A). In Sec. 6, we also show that finetuning consistently improves state prediction accuracy.

3.7. Object Discovery

Given many observation of how users interact with objects in a new scene, we propose a simple method to discover common object categories. First, we predict the active hand segments which is typically over-segmented. Then, we calculate segment-base feature \bar{f} as the average of the frame-based features and apply a hierarchical clustering method using cosine similarity to group similar segments into clusters. By assuming that the same object category is interacted by hands multiple-times in a similar way, two similar active hand segments likely corresponds to the same object categories. In Sec. 6.3, we show that our HandCam system can discover categories more accurately than the classical HeadCam system.

3.8. Combining HandCam with HeadCam

Despite the inferior recognition accuracy from HeadCam, it has some unique properties which motivate us to combine the strength of both cameras. Firstly, sometimes HandCam is occluded by other objects, whereas HeadCam keeps a clear view of the hands (Fig. 6(a)) due to required hand-eye coordination. We propose to concatenate frame-based features of both HeadCam and HandCam to achieve the best recognition accuracy. Moreover, HeadCam observed more scene information such that Structure-from-Motion can be applied to approximately recover user’s 3D

trajectory. Utilizing HeadCam, we can visualize human behavior in 3D as shown in Fig. 6(b).

4. Dataset

We have collected one of the first “HandCam” video data. Our dataset contains 20 round of data collection (60 video sequences), where each round consists of three synchronized video sequences (two from HandCam and one from HeadCam). In total, our dataset contains ~ 115.5 minutes of videos, which is at a similar scale of the egocentric video dataset [5]. Our dataset will be publicly available¹.

In order to thoroughly analyze tasks involving recognizing object category, hand gesture, etc., we explicitly collect videos in multiple indoor scenes, interacting with multiple object categories, and multiple object instances within each category. Moreover, we ask multiple users to wear our system in a casual way to consider the variation introduced by multiple users. A thorough statistics is shown in Table. 7. We summarize the properties of our dataset below.

- **Scene:** We have collected videos in three scenes: a small office, a mid-size lab, and a large home (Fig. 6(b)), where office and lab involve many similar object interaction, but involve very different object interaction as in home.
- **Task:** We pre-define a number of tasks for users to follow. To increase variation, each user randomly selects a task-order to perform.
- **Object category:** For many object categories², we prepare many instances so the instances are separable in our train/test splits.
- **User:** We have 11 unique users involved in collecting the videos.
- **Ground truth states:** we ask users to consider both HandCams and HeadCam to decide the ground truth state at each moment in time. For instance, both examples in Fig. 2(b) are in active state.

Training v.s. testing set. We have two settings. Firstly, we train on office and lab. Then, we test on home. We refer this as “Home” setting. This is a challenging setting, since home is an unseen scene and there are many unseen object categories and activities. In the second setting, we evenly divide the video sequences into half for training and the remaining half for testing in all scenes. We refer this as “AllScenes” setting.

¹Please find a subset of videos <https://www.youtube.com/watch?v=ZAlhKnEhCjY>.

²Typically movable objects such as toys, kettles, cups, bottles, cookies, coins, cellphones, rulers, pens, books, and magnets.

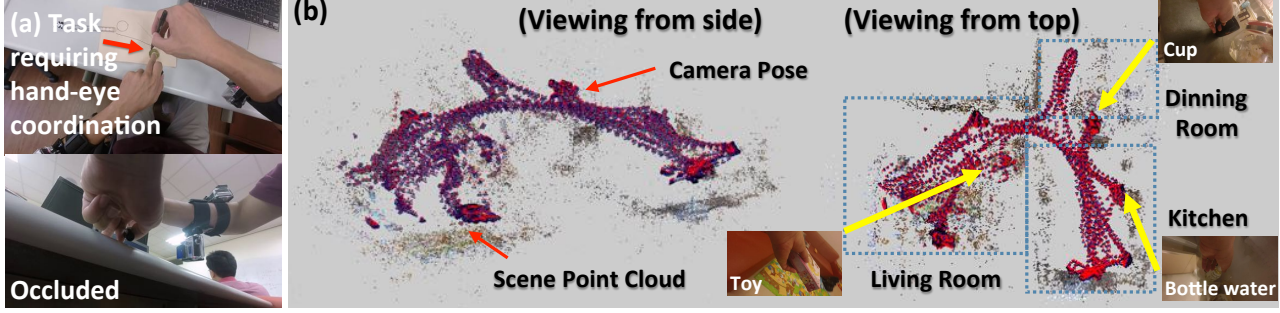


Figure 6: Panel (a) shows an example where HandCam (bottom) is occluded but HeadCam (top) observed the activity requiring hand-eye coordination. Panel (b) shows 3D Structure of the Scene reconstructed from HeadCam imgs. A pair of blue and red dots indicates the recovered camera 3D pose and other color-coded dots show the color of the scene. Since HeadCam and HandCams are synchronized, our system knows roughly the corresponding 3D location of each states in time.

	# Vid.	# Fra.	# Users	#TO	#Cat.	#Inst.	#Gest.	Categories Instances
Office	6	7213	6	1	6	30	10	lamp switch 1; whiteboard pen 6; thermos bottle 5; book 6; computer 6; magnet 6
Lab	8	9299	8	3	9	58	11	whiteboard eraser 1; computer 7; cellphone 8; coin 4; ruler 8; thermos bottle 7; whiteboard pen 7; pen 8; cup 8
Home	6	11390	4	3	12	35	11	TV remote 1; AC remote 1; switch 1; window 1; fridge 1; cupboard 1; water tap 1; toy 4; kettle 6; cup 6; bottle 6; snack 6
Total	20	27902	11	7	23	111	12	

Figure 7: Statistics of our HandCam dataset. Vid. stands for videos. Fra stands for frames. TO stands for task-order. Cats. stands for categories. Inst. stands for instances. Gest. stands for gestures.

5. Implementation Detail

Camera system. Our system consists of three GoPro 3+ cameras to record videos with 1920x1080 resolution and we process them at 6 fps. In order to record synchronized video sequences among two HandCam and one head-mounted camera, we use the GoPro Wi-Fi remote control to start and end recording all three cameras at the same time.

Alignment. We set $\beta^{th} = 40$ and achieve stable hand alignment results. We also try seven scales (i.e., [0.9, 1, 1.1, 1.2, 1.3, 1.4, 1.5]) in our multi-scales alignment method.

Training. We set SVM regularization parameters, parameter d of state change features, and λ automatically using 5-fold cross-validation for each setting. We finetune an imagenet pre-trained Alexnet on our dataset using the following parameters consistently for all tasks: maximum iterations = 40000, step-size = 10000, momentum = 0.9, every 1000 iteration weight decay = 0.1, and learning rate = 0.001. To augment our dataset, we flip the left HandCam frames horizontally and jointly trained with the right HandCam frames.

6. Experiment Results

We evaluate three state recognition tasks: free v.s. active, gesture, and object category recognition. Some tasks are conducted in two train/test settings: Home and AllScenes as described in Sec. 4. In addition, a challenging object discovery task is evaluated in Home setting. All the following

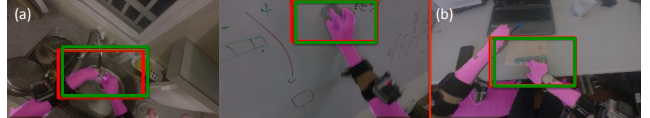


Figure 8: Typical hand segmentation and manipulation region prediction. Panel (a) shows two good examples. The prediction and ground truth are shown in green boxes and red boxes, respectively. Panel (b) shows a typical hand mask mistake where the wooden floor with skin-like color is segmented as hands. When the mistake is not significant, the predicted manipulation region can still be correct.

experiments are conducted using fc6 features in Alexnet.

HeadCam baseline. We apply state-of-the-art hand segmentation method [15] (pink masks in Fig. 8) to predict manipulation region (green boxes in Fig. 8) at each frame. Similar to [17], we predict at most two boxes, one for left and one for right hands. Fig. 8 shows the ground truth in [15]. red boxes. Note that we artificially increase the systems accuracy by manually labeling many hand masks in our dataset for training hand segmentation method [15]. Please see Appendix B for more detail. Next, we crop the HeadCam images with respect to the predict manipulation region and apply the same methods introduced in this paper to recognize hand states.

Method abbreviation. To facilitate discussion, we introduce the following abbreviations for different methods. BL

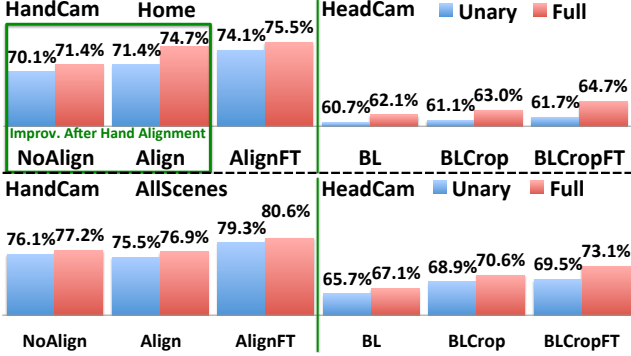


Figure 9: Free v.s. active recognition accuracy. Top-row shows the global accuracy in Home. Bottom-row shows the global accuracy in AllScenes. In all plots, blue bar denotes frame-based classification. Red bar denotes our full model.

is HeadCam baseline without cropping image using pre-trained feature. BLCrop is HeadCam baseline with manipulation region crop using pre-trained feature. BLCropFT is BLCrop using finetuned feature. NoAlign is HandCam no hand alignment using pre-trained feature. Align is HandCam with alignment using pre-trained feature. AlignFT is Align using finetuned feature.

6.1. Free v.s. Active Recognition

Free v.s. active recognition accuracy (acc.) comparison is shown in Fig. 9, where top-row shows the acc. in Home and bottom-row shows acc. in AllScenes.

Pre-trained CNN. Using pre-trained CNN feature, our full method (74.7% acc. in Home and 76.9% acc. in AllScenes) is already significantly better than both the non-cropped (62.1% acc. in Home and 67.1% acc. in AllScenes) and cropped (63% acc. in Home and 70.6% acc. in AllScenes) HeadCam baselines. These results confirm that HandCam is a great alternative to classical HeadCam systems.

Unary v.s. Full. Our full model also consistently outperforms frame-based unary model in all settings and for both HandCam and HeadCam (with the best improvement of 3.3% in Home and aligned HandCam setting).

Hand Alignment. Although in AllScenes, hand alignment shows no critical improvement. However, in the challenging Home setting, we confirm that hand alignment improves acc. by 3.3% from 71.4% to 74.7% (full model+pre-trained feature in green box of Fig. 9). This implies that hand alignment might be critical in practical cross-scenes usage.

Finetune CNN. Finetuning CNN shows consistent improvement in all settings and for both HandCam and HeadCam. Our finetuned full method achieves 75.5% acc. in Home and 80.6% acc. in AllScenes which is 10.8% and 7.4% better than the finetuned cropped baseline (64.7% acc. in Home and 73.1% acc. in AllScenes).

6.2. Gesture Recognition

Gesture recognition accuracy comparison is shown in Fig. 10. Gesture recognition is more challenging than free v.s. active recognition, since it needs to classify 12 + 1 (free

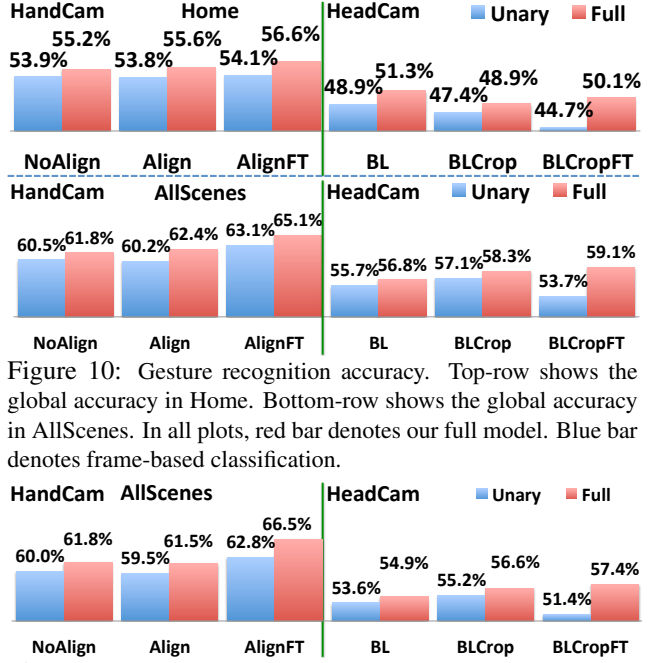


Figure 10: Gesture recognition accuracy. Top-row shows the global accuracy in Home. Bottom-row shows the global accuracy in AllScenes. In all plots, red bar denotes our full model. Blue bar denotes frame-based classification.

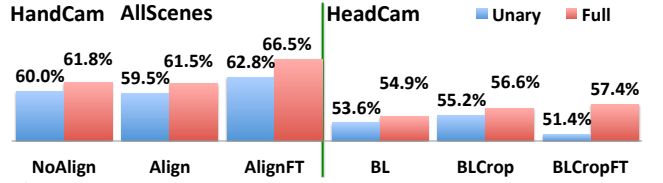


Figure 11: Object category classification comparisons in AllScenes. In all plots, red bar denotes our full model. Blue bar denotes frame-based classification.

hand state) gestures. However, gesture recognition shares the same trend in free v.s. active recognition. Except that, in Home setting, hand alignment only shows 0.4% acc. improvement using pre-trained feature. Nevertheless, our finetuned full method achieves 56.6% acc. in Home and 65.1% acc. in AllScenes which is 6.6% and 6% better than the finetuned cropped baseline (50.1% acc. in Home and 59.1% acc. in AllScenes).

6.3. Object Category Recognition

Object category recognition accuracy comparison in AllScenes setting is shown in Fig. 11. Object category recognition is more challenging than gesture recognition, since it needs to classify 23 + 1 (free hand state) categories. However, it shares the same trend in free v.s. active recognition. Most importantly, our finetuned full method achieves 66.5% acc. which is 9.1% better than the finetuned cropped baseline (57.4% acc.). In Home setting, since many object categories are not observed in training, we evaluate the following object discovery task.

Category Discovery. We treat object category discovery as a clustering task, and compare the clustering results between our best HandCam configuration (i.e., AlignFT for free v.s. active recognition) and the best HeadCam configuration (i.e., BLCropFT for free v.s. active recognition). We report a modified purity (similarly defined in [27]) to focus on discovering object categories (not free-hand) as described below. For all frames in each cluster, we obtain their ground truth object labels and calculate the dominate label. If the dominate label is not hand-free state, we count the number of discovered frames as the number of ground truth

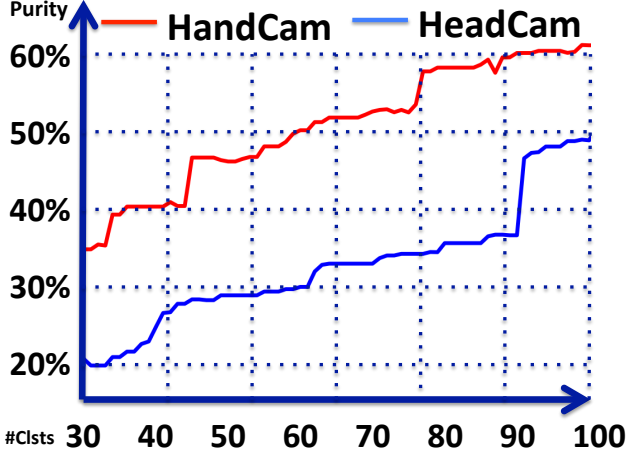


Figure 12: Purity for Object Category Discovery. Our HandCam (red curve) consistently outperforms HeadCam (blue curve) by about 10% from 30 to 100 clusters.

labels equals the dominate label. This number is accumulated across all clusters. Then, the purity is the total number of discovered frames divided by the number of true active-hand frames. We calculate the purity with different number of clusters in Fig. 12. We confirm again that HandCam significantly outperforms HeadCam by about 10% from 30 to 100 clusters.

6.4. Combining HandCam with HeadCam

We show comparison among HeadCam best configuration (i.e., cropped with finetuned feature), HandCam best configuration (i.e., aligned hand with finetuned feature), and HandCam+HeadCam (finetuned feature concatenation) in Fig. 14. HandCam+HeadCam achieves the best accuracy consistently in three tasks: FvsAHome stands for free v.s. active recognition in Home, GesAll stands for gesture recognition in AllScenes, and ObjAll stands for object category recognition in AllScenes. In particular, HandCam+HeadCam achieves a $\sim 3\%$ improvement on the FvsAHome task.

6.5. Qualitative Results

We show typical examples in Fig. 13. Notice that our HandCam system is robust even when there is no hand-eye

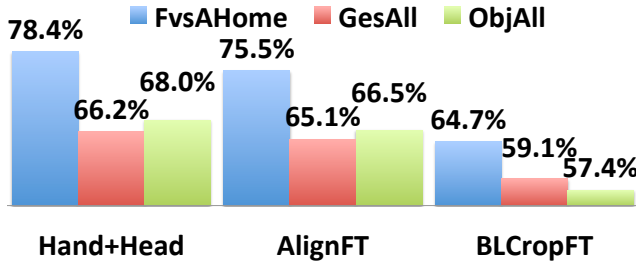


Figure 14: Comparing HandCam+HeadCam with HandCam (AlignFT) and HeadCam (BLCropFT) in three tasks: FvsAHome stands for free v.s. active recognition in Home, GesAll stands for gesture recognition in AllScenes, and ObjAll stands for object category recognition in AllScenes.

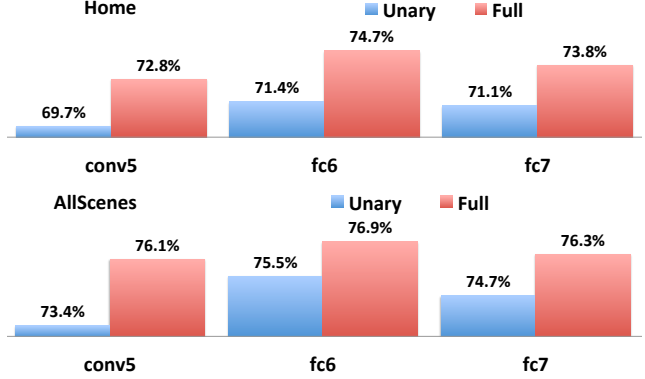


Figure 15: Free v.s. active recognition accuracy comparison among three CNN architectures: conv5, fc6, and fc7. Top-row shows the global accuracy in Home. Bottom-row shows the global accuracy in AllScenes. In all plots, blue bar denotes frame-based classification. Red bar denotes our full model.

coordination.

7. Conclusion

We propose a novel HandCam system for recognizing various hand states. To evaluate our system, we collect one of the first dataset with both HandCam and HeadCam observing multiple object categories, instances, gestures in multiple scenes. Our HandCam significantly outperforms a state-of-the-art HeadCam system in all tasks by at most 10.8% improvement in accuracy. We also observe that fine-tuning CNN significantly improves accuracy (at most 4.9% acc. improvement). Most importantly, we show that combining HandCam with HeadCam gives the best performance in many tasks. In the future, we will study how to jointly design HandCam and HeadCam.

Appendices

A. Deep Feature

We train three different CNN architectures: a 5-layers convolution model (conv5), a 6-layers with last fully-connected layer (fc6), and a 7 layers with last 2 fully-connected layers (fc7)³. Their performances on free v.s. active recognition in Home and AllScenes settings using unary and our full models are show in Fig. 15. Our results show that a compact six layers model (fc6) achieves the best accuracy, while being more computationally efficient than the original Alexnet [14].

B. HeadCam Baseline

We first test the pre-trained hand segmenter [15] but find the pre-trained model does not generalize well to images

³All architectures have an additional softmax layer at the end.

(a) Home **Time line** 

HandCam									
HandCam	RC-AC	Bottle	Cookie	Toy	Cupboard	Kettle			
HandCam	T-4-F	L-D	F	L-D	P-E	T-4-F	M-W		
HeadCam									
HeadCam	RC-AC	F	F	F	Cookie	Toy	F	F	Kettle
HeadCam	T-4-F	F	F	F	L-D	F	T-4-F	F	M-W

(b) Lab **HandCam Occluded**

HandCam							
HandCam	W-E	Cellphone	Pen	Cup	T-B	Cup	
HandCam	L-D	T-4-F	F	L-D	L-D	L-D	
HeadCam							
HeadCam	F	Computer	Pen	F	T-B	T-B	F
HeadCam	L-T	L-D	T-4-F	L-T	F	L-D	L-D

(c) Office **HandCam Occluded**

HandCam						
HandCam	Book	T-B	computer	computer	W-P	T-B
HandCam	F	L-D	P-E	F	L-T	L-D
HeadCam						
HeadCam	F	F	F	F	W-P	F
HeadCam	F	F	F	F	L-T	F

Figure 13: Typical examples of predicted object categories (white font) and gestures (black font). Panel (a,b,c) show the comparison between HandCam (top-row) and HeadCam (bottom-row) in home, lab, and office scenes, respectively. Prediction errors are highlighted in red background. T-B is thermos-bottle. M-W is medium-wrap. W-P is whiteboard-pen. W-E is whiteboard-eraser. RC-TV is remote-control-TV. RC-AC is remote-control-AC. L-D is large-diameter. L-T is lateral-tripod. T-4-F is thumb-4-finger. F is free. P-E is parallel-extension. We block a few regions in the images to avoid privacy concerns. HeadCam often makes wrong prediction when there is no hand-eye-coordination. Our HandCam sometimes makes wrong prediction when the camera is occluded.

in our dataset. In order to build a strong HeadCam baseline, we label the hand masks in one video per scene and retrain the hand segmenter. We take a similar approach as in [17] to predict the manipulation region (i.e., a bounding box) of each hand (i.e., both left and right hands) at each frame. In detail, we use a 10 nearest neighbor approach to retrieve the top 10 frames in our database with similar hand mask as the query hand mask. Given the top 10 frames and their corresponding ground truth manipulation regions (i.e., boxes containing hands and objects), we use mean-shift to find the mode of the manipulation region, and use the mode region as the predicted region. In order to build a strong baseline, for each query frame, we use all frames of other videos in the same scene as frames in our database. We treat the manipulation region prediction task as an object detec-

tion task, and measure the overlap between the predicted region and ground truth region. We consider the prediction to be correct, if the overlap is more than a threshold. In Fig. 16, we evaluate the percentage of correct prediction of the detection task at different thresholds. Our results show that manipulation region prediction is not perfect, even we have intentionally tried to improve its performance.

References

- [1] A. Betancourt, M. Lopez, C. Regazzoni, and M. Rauterberg. A sequential classifier for hand detection in the framework of egocentric vision. In *CVPRW*, 2014.
- [2] J. Canny. A computational approach to edge detection. *PAMI*, PAMI-8(6):679–698, 1986.
- [3] L. Chan, Y.-L. Chen, C.-H. Hsieh, R.-H. Liang, and B.-Y. Chen. Cyclopsring: Enabling whole-hand and context-aware

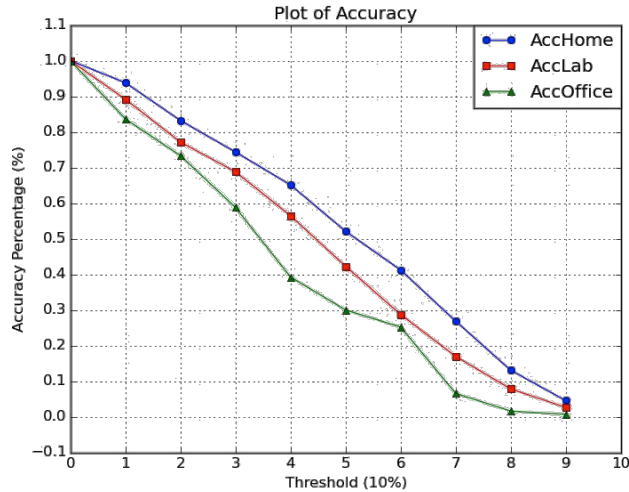


Figure 16: Manipulation region prediction performance in Average Precision (Y-axis) with different overlap threshold (X-axis) for three scenes: home, office, and lab.

interactions through a fisheye ring. In *UIST*, 2015.

- [4] D. Damen, A. Gee, W. Mayol-Cuevas, and A. Calway. Egocentric real-time workspace monitoring using an rgb-d camera. In *IROS*, 2012.
- [5] D. Damen, T. Leelasawassuk, O. Haines, A. Calway, and W. Mayol-Cuevas. You-do, i-learn: Discovering task relevant objects and their modes of interaction from multi-user egocentric video. In *BMVC*, 2014.
- [6] F. De la Torre, J. K. Hodgins, J. Montano, and S. Valcarcel. Detailed human data acquisition of kitchen activities: the cmu-multimodal activity database (cmu-mmac). In *Workshop on Developing Shared Home Behavior Datasets to Advance HCI and Ubiquitous Computing Research, in conjunction with CHI 2009*, 2009.
- [7] A. Fathi, A. Farhadi, and J. M. Rehg. Understanding egocentric activities. In *ICCV*, 2011.
- [8] A. Fathi, Y. Li, and J. M. Rehg. Learning to recognize daily actions using gaze. In *ECCV*, 2012.
- [9] A. Fathi and J. M. Rehg. Modeling actions through state changes. In *CVPR*, 2013.
- [10] A. Fathi, X. Ren, and J. M. Rehg. Learning to recognize objects in egocentric activities. In *CVPR*, 2011.
- [11] J. Ghosh, Y. J. Lee, and K. Grauman. Discovering important people and objects for egocentric video summarization. In *CVPR*, 2012.
- [12] D.-A. Huang, W.-C. Ma, M. Ma, and K. M. Kitani. How do we use our hands? discovering a diverse set of common grasps. In *CVPR*, 2015.
- [13] D. Kim, O. Hilliges, S. Izadi, A. D. Butler, J. Chen, I. Oikonomidis, and P. Olivier. Digits: Freehand 3d interactions anywhere using a wrist-worn gloveless sensor. In *UIST*, 2012.
- [14] A. Krizhevsky, I. Sutskever, and G. E. Hinton. Imagenet classification with deep convolutional neural networks. In F. Pereira, C. Burges, L. Bottou, and K. Weinberger, editors, *NIPS*, 2012.
- [15] C. Li and K. M. Kitani. Model recommendation with virtual probes for egocentric hand detection. In *ICCV*, 2013.
- [16] C. Li and K. M. Kitani. Pixel-level hand detection in egocentric videos. In *CVPR*, 2013.
- [17] Y. Li, A. Fathi, and J. M. Rehg. Learning to predict gaze in egocentric video. In *ICCV*, 2013.
- [18] Y. Li, Z. Ye, and J. M. Rehg. Delving into egocentric actions. In *CVPR*, 2015.
- [19] Z. Lu and K. Grauman. Story-driven summarization for egocentric video. In *CVPR*, 2013.
- [20] M. Moghimi, P. Azagra, L. Montesano, A. C. Murillo, and S. Belongie. Experiments on an rgb-d wearable vision system for egocentric activity recognition. In *CVPR Workshop on Egocentric (First-person) Vision*, Columbus, OH, 2014.
- [21] K. Ohnishi, A. Kanehira, A. Kanezaki, and T. Harada. Recognizing activities of daily living with a wrist-mounted camera. *CoRR*, abs/1511.06783, 2015.
- [22] H. Pirsiavash and D. Ramanan. Detecting activities of daily living in first-person camera views. In *CVPR*, 2012.
- [23] G. Rogez, J. S. S. III, M. Khademi, J. M. M. Montiel, and D. Ramanan. 3d hand pose detection in egocentric RGB-D images. *CoRR*, abs/1412.0065, 2014.
- [24] G. Rogez, J. S. S. III, and D. Ramanan. First-person pose recognition using egocentric workspaces. In *CVPR*, 2015.
- [25] A. Saxena, J. Driemeyer, and A. Y. Ng. Robotic grasping of novel objects using vision. *Int. J. Rob. Res.*, 27(2):157–173, 2008.
- [26] M. Sun, A. Farhadi, B. Taskar, and S. Seitz. Salient montages from unconstrained videos. In *ECCV*, 2014.
- [27] Tan, Steinbach, and Kumar. Introduction to data mining. 2005.
- [28] A. Vardy, J. Robinson, and L.-T. Cheng. The wristcam as input device. In *ISWC*, 1999.